



HAL
open science

In situ study of the crystallization mechanism in LiNbO₃-SiO₂ glasses

Hélène Vigouroux, Evelyne Fargin, Bruno Le Garrec, Marc Dussauze, Vincent Rodriguez, Frédéric Adamietz, Johann Ravaux, Renaud Podor, Sergei Lotarev, Vladimir Sigaev, et al.

► To cite this version:

Hélène Vigouroux, Evelyne Fargin, Bruno Le Garrec, Marc Dussauze, Vincent Rodriguez, et al.. In situ study of the crystallization mechanism in LiNbO₃-SiO₂ glasses. Physics and Chemistry of Glasses - European Journal of Glass Science and Technology Part B, 2013, 54 (2), pp.84-88. hal-00826451

HAL Id: hal-00826451

<https://hal.science/hal-00826451>

Submitted on 26 Jul 2022

HAL is a multi-disciplinary open access archive for the deposit and dissemination of scientific research documents, whether they are published or not. The documents may come from teaching and research institutions in France or abroad, or from public or private research centers.

L'archive ouverte pluridisciplinaire **HAL**, est destinée au dépôt et à la diffusion de documents scientifiques de niveau recherche, publiés ou non, émanant des établissements d'enseignement et de recherche français ou étrangers, des laboratoires publics ou privés.

In situ study of the crystallization mechanism in LiNbO₃–SiO₂ glasses

Hélène Vigouroux,^{*1,2} Evelyne Fargin,¹ Bruno Le Garrec,² Marc Dussauze,³ Vincent Rodriguez,³ Frédéric Adamietz,³ Johann Ravoux,⁴ Renaud Podor,⁴ Sergei Lotarev,⁵ Vladimir Sigaev,⁵ Dominique Vouagner,⁶ Dominique De Ligny⁶ & Bernard Champagnon⁶

¹ CNRS, Université de Bordeaux, ICMCB, 87 avenue du Dr. A. Schweitzer, Pessac, F- 33608, France

² CEA-CESTA, 15 avenue des Sablières, 33114 Le Barp, France

³ Institut des Sciences Moléculaires – UMR 5255 CNRS, Université Bordeaux, 351 cours de la Libération, 33405 Talence, France

⁴ Institut de Chimie Séparative de Marcoule, UMR 5257 CEA-CNRS-UM2-ENSCM Site de Marcoule, Bat 426, BP 17171, F-30207 Bagnols sur Cèze cedex

⁵ Mendeleev University of Chemical Technology of Russia, Miusskaya pl.9, 125047 Moscow, Russia

⁶ Université Claude Bernard Lyon-1, LPCML-UMR 5620 CNRS, 12 rue Ada Byron, 69662 Villeurbanne, France

A crystallization study of lithium niobium silicate glass with the molar composition 35Li₂O.25Nb₂O₅.40SiO₂ is reported using in situ techniques (x-ray diffraction, Raman spectroscopy and environmental electron microscopy) at high temperatures. Those techniques reveal that the surface crystallization begins at T_g with c-axis crystallites oriented perpendicular to the surface. Precipitation of nuclei, followed by growth and coalescence processes, induce the formation of particles and spherulites 0.5–4 μm diameter in size. A strong difference between surface and bulk crystallization has been observed with bulk crystallization yielding to 30 μm diameter size spherulites. Those original spherulite shapes could be the origin of the macroscopic bulk second harmonic generation (SHG) signal.

1. Introduction

Glass ceramics with a precipitated ferroelectric crystalline phase are of interest for many applications because of their dielectric and electro-optic properties.^(1,2) The development of such transparent glass-ceramics with ferroelectric properties is required for optical applications. They can be prepared through bulk controlled precipitation of non-centrosymmetric submicroscopic crystals.

Within the family of ferroelectric crystalline phases, crystalline lithium niobate possesses a large second order nonlinear optical (NLO) response.^(3,4) It is widely used for frequency conversion in laser fabrication. The precipitation of crystalline lithium niobate particles in Li₂O/Nb₂O₅/SiO₂ glass has been widely studied.^(5–10) Depending on the heat treatment consisting of a nucleation step followed by crystal growth step, surface and/or bulk crystallization of the LiNbO₃ crystalline phase has been observed. X-ray diffraction together with second harmonic generation (SHG) measurements have revealed a c-axis orientation of surface crystallized particles, whereas this orientation is less pronounced in the bulk sample. A translucent glass-ceramic sample has

been produced for which the Maker fringes pattern recorded in transmission mode reveals a strong and reproducible SHG signal with a maximum intensity at normal incidence.⁽¹⁰⁾

In this paper, we will report an *in situ* crystallization study of this particular glass composition. The surface crystallization process will be studied using X-Ray diffraction, Raman and scanning electron microscopy in conjunction with high temperature devices. Both similarities and differences between the surface and bulk crystallization mechanism will be identified and discussed.

2. Experimental procedure

2.1 Glass processing

Glasses with the composition (mol%) 35Li₂O–25Nb₂O₅–40SiO₂ (called LNS 25) were prepared using Li₂CO₃ (Merck, 99%), Nb₂O₅ (Alfa Aesar 99.9%) and SiO₂ (Alfa Aesar, 99.8%). All batches (~20 g) were prepared by a conventional melt quenching method. Melting was performed in ambient atmosphere in a platinum crucible at 1450°C for 30 min. Then, the melts were rapidly quenched at room temperature by pouring onto a stainless steel plate and pressing by another plate to obtain samples with an approximate final thickness of 1 mm. The glasses were annealed for 15 h at 510°C (70°C below the glass transition

* Corresponding authors. Email vigouroux@icmcb-bordeaux.cnrs.fr; fargin@icmcb-bordeaux.cnrs.fr

Presented during the International Conference on the Chemistry of Glasses and Glass-Forming Melts, Oxford, September 2011

temperature) to remove internal stresses. Then they were slowly cooled to room temperature with a 1°C/min cooling rate. The obtained glass plates are x-ray amorphous and have been polished to be optically transparent.

2.2 X-ray diffraction

X-ray diffractometry was carried out using a PANalytical X'pert MDP (Co K_{α} at 1.78897 Å) in a θ - θ Bragg-Brentano geometry equipped with a Fe filter (working voltage and intensity were 35 kV and 30 mA, respectively). The sample temperature was controlled using an Anton Paar HTK12 cell.

The sample was polished with a final thickness of 0.3 mm for this *in situ* analysis. Then it was rapidly heated (60°C/min) from room temperature to 500°C in order to avoid an excess of nuclei precipitating before the nucleation step.⁽¹⁰⁾ Then the sample was heat treated with a 20°C/min heating rate from 500 to 580°C, and the sample temperature was held at 580°C for 1 h. Finally, the sample was heated up to 750°C at a 10°C/min heating rate. X-ray diffractograms were recorded each 20°C step from 560 to 750°C. The θ angular domain ranged from 24 to 75°, and the recording time for one diffractogram was 10 min.

2.3 Raman spectroscopy

High temperature *in situ* Raman spectra were collected using an Aramis micro spectrometer (Horiba). The sample was heated in a platinum crucible with a temperature controlled Linkam stage TS1500. To prevent any overlap of the Raman spectra by the black body emission, a UV He/Cd laser (Kimmon) at 325 nm was used. With a UV objective $\times 10$ the laser power on the sample was 1.6 mW and the spot size diameter was 1.6 mm. The 2400 l/mm grating allowed a spectral resolution of 2 cm^{-1} . Typical spectra were collected for 60 s to ensure a good signal noise ratio.

The sample was rapidly heat treated from room temperature to 580°C with a 60°C/min heating rate then the sample temperature was held for 1 h. This heating rate was used to avoid additional nucleation before this temperature and to only focus on the crystallization induced during the isothermal treatment.

2.4 Environmental scanning electron microscopy

A FEI Quanta 200 ESEM FEG equipped with a 1000°C hot stage was used to perform the *in situ* experiments. The sample was heated to the desired temperature at a 10°C/min heating rate. During the sample heating, images were regularly recorded in order to observe crystal formation and growth. Complementary images were also recorded after sample cooling at room

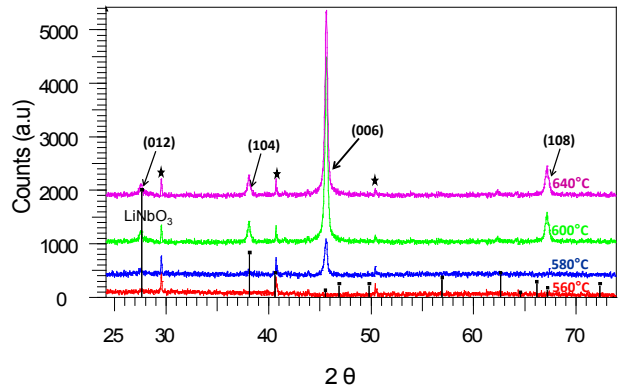


Figure 1. X-ray diffractograms of LNS 25 glasses recorded at different temperatures during *in situ* experiments. XRD lines of Al_2O_3 (*) correspond to the alumina sample crucible. Indexing for LiNbO_3 are indicated on the XRD (lines with filled square on their top- JCPDS 00-020-0631). Arrows specify the particular Bragg diffraction peaks of the LNS 25 glass-ceramic [In colour online]

temperature or on preheated samples. These complementary images are referred to as “*ex situ*” images.

3. Results and discussion

The x-ray diffractograms recorded at different temperatures (560, 580, 600 and 640°C) are shown in Figure 1. The x-ray diffractograms recorded above 640°C are all roughly identical to the one recorded at $T=640^\circ\text{C}$. Thus, they are not shown in Figure 1.

The peaks that are present at $2\theta=29.5^\circ$, 41° , 44° and 50.5° on all x-ray diffractograms correspond to the alumina crucible. As a consequence, no diffraction line corresponding to a crystalline phase is observed on the x-ray diffractogram recorded at 560°C. The first peak (centred at 46°) appears on the pattern recorded at $T=580^\circ\text{C}$. This diffraction line can be attributed to the (006) lattice plane of the LiNbO_3 crystalline phase. Increasing the temperature up to 600°C leads to both an increase in the intensity of the LiNbO_3 (006) diffraction line and to the presence of additional x-ray diffraction (XRD) lines, centred at 27.5° , 38° and 67° , that can be respectively attributed to the (012), (104) and (108) lattice planes of the LiNbO_3 structure. No significant change in the XRD patterns recorded above $T=600^\circ\text{C}$ is observed. The experimental $\rho=I_{(006)}/I_{(012)}$ ratio values determined from the intensities of the (006) and (012) diffraction lines recorded at $T\geq 600^\circ\text{C}$ is significantly higher ($\rho\sim 13$) than the ratio determined from a x-ray diffractogram corresponding to the isotropic LiNbO_3 powder where $\rho\sim 0.03$ (see Figure 1). The increase of the ρ ratio is attributed to a preferential orientation of the LiNbO_3 crystallites along the c -axis which remains perpendicular to the glass surface.⁽⁸⁻¹⁰⁾ The intensity increase of the (006) peak when $T>580^\circ\text{C}$ reveals an accumulation of c -crystallites perpendicular to the surface. Furthermore, the appearance of the other

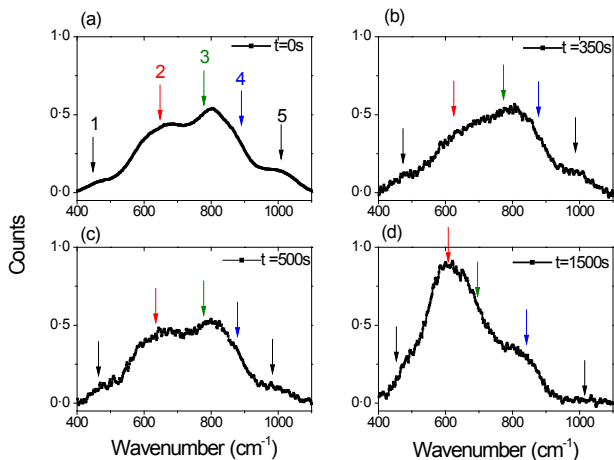


Figure 2. Raman spectra of LNS 25 glass performed in situ. Time $t=0$ s indicates the beginning of the experiment and corresponds to the Raman spectrum recorded at room temperature before heating the sample. At $t=330$ s, the sample has reached $T=580^\circ\text{C}$. The spectra recorded at $t=500$ s and 1500 s correspond to an isothermal heating of the sample at $T=580^\circ\text{C}$. The arrows indicate the band positions (1 & 5=silicate network vibrations, 2=stretching vibration of Nb–O–Nb bridges in a 3D network of regular NbO₆ octahedra, 3=stretching vibration of Nb–O–Nb bridges but in distorted NbO₆ octahedra, 4=Nb–O stretching modes of distorted NbO₆ octahedra sharing at least one corner with SiO₄ tetrahedra.) [In colour online]

peaks, the intensity of which remains low, points out that the c -axis of the crystallites is not perfectly oriented perpendicularly to the surface.

In situ μ -Raman measurements were recorded on a glass sample from room temperature to the glass transition temperature in order to investigate the local structural modifications due to the crystallization process. Four representative Raman spectra recorded as function of temperature and time (that have been normalized to same area value) are shown in Figure 2.

Five vibrational bands are present in all the recorded spectra. They can be assigned as follows. Bands 1 and 5, respectively, centred at 420–480 and 980–1200 cm^{-1} , are attributed to the silicate network.^(11–13) Band 2, centred at 610–650 cm^{-1} , can be assigned to the stretching vibration of Nb–O–Nb bridges in a 3D network of regular NbO₆ octahedra.^(14,15) It is also observed in the LiNbO₃ crystalline phase.^(16–20) Band 3, centred at 695–780 cm^{-1} , is assigned to the stretching vibration of Nb–O–Nb bridges but in distorted NbO₆ octahedra.⁽²¹⁾ Band 4 which is centred at 840–890 cm^{-1} is attributed to the Nb–O stretching modes of the distorted NbO₆ octahedra sharing at least one corner with SiO₄ tetrahedra.^(12–15) Hence, this band is characteristic of the LNS 25 glass.

During the sample heating and isothermal treatment at $T=580^\circ\text{C}$, the intensities of bands 3 and 4 decrease in a regular fashion with temperature and time relative to the intensity of band 2. This corresponds

to a rearrangement of the distorted NbO₆ octahedra and it indicates that the niobate network becomes progressively more regular with temperature and soaking time. These intensity modifications are clearly characteristic of the formation of the LiNbO₃ crystallites. The crystallization process occurring at the glass transition temperature (580°C) corresponds to a very fast process: after an 1170 s isothermal heat treatment of the sample at $T=580^\circ\text{C}$ (i.e. for $t=1500$ s) the recorded Raman spectra remain unchanged. In parallel, bands 1 and 5 that are characteristic of the silicate network have relatively almost disappeared compared to the crystal bands, probably due to the higher Raman cross section intensity of LiNbO₃. We might expect UV assisted crystallization.

One must note that during the thermal treatment of the samples up to 580°C (Figure 2(a) to (d)), the bands shift towards higher wavelengths due to thermal expansion.

The environmental scanning electron microscope equipped with a high temperature stage (HT-ESEM) allows *in situ* observation of the microstructural modifications due to the crystallization process. The information obtained using this technique will be complementary with previously reported HT- μ -Raman and HT-XRD data. Characteristic micrographs of the microstructural modifications occurring on the LNS 25 glass surface as function of temperature (sample heat treatment is performed at $10^\circ\text{C}/\text{min}$ heating rate) are reported in Figure 3. From room temperature up to approximately 550°C , the glass remains homogeneous (Figure 3(a)). Then, the crystallites begin to precipitate and 300 nm diameter grains are observed at $T=554^\circ\text{C}$ (Figure 3(b)). At $T=572^\circ\text{C}$, (Figure 3(c)), the crystallites agglomerate into 1 μm diameter spherulite arrangements. When $T=577^\circ\text{C}$ (Figure 3(d)) (i.e. just below the glass transi-

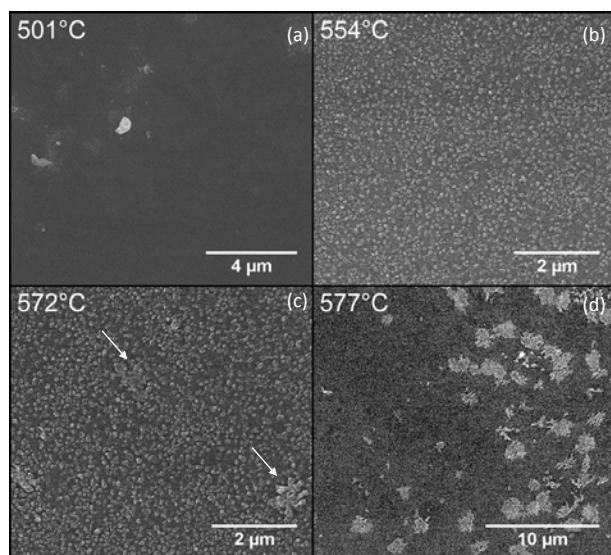


Figure 3. In situ HT-ESEM images recorded on the LNS 25 glass

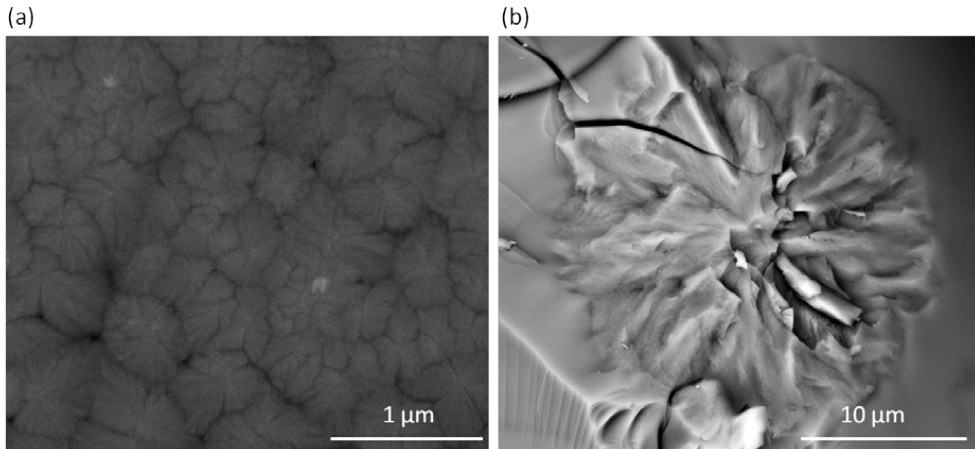


Figure 4. ESEM images recorded *ex situ* on (a) the surface of the LNS 25 glass after heat treatment at $T=850^{\circ}\text{C}$ and cooling to room temperature and on (b) the bulk of the LNS 25 glass after heat treatment at $T=590^{\circ}\text{C}$, followed by cooling to room temperature and fracture of the sample

tion temperature), the size of the spherulites increases and reaches $3\ \mu\text{m}$ diameter. At higher temperatures the number of such spherulites is also increased. According to these *in situ* HT-ESEM observations of the crystallization process, a two step mechanism can be proposed corresponding to precipitation of the crystallites followed by a coalescence process leading to the formation of spherulites.

One should also notice that crystallization occurs before the glass transition temperature (i.e. 580°C) during the *in situ* HT-ESEM experiments, contrary to what has been observed during the Raman or x-ray diffraction experiments. One hypothesis that can be proposed to explain this earlier crystallization lies in the fact that ESEM experiments have been performed under low pressure (300 Pa) – whilst the HT-XRD and HT- μ -Raman experiments have been performed under atmospheric pressure. Fuss *et al* have reported that lowering the pressure results in crystallization and nucleation at lower temperatures.⁽²²⁾

A LNS 25 glass-ceramic sample has been observed after *in situ* heat treatment from 20 up to 850°C in the HT-ESEM chamber and cooling to room temperature (Figure 4(a)). Another LNS 25 glass-ceramic sample has also been prepared by heating the glass in the temperature range $520\text{--}590^{\circ}\text{C}$ for 135 min. Then, this sample has been cut into two parts in order to investigate the bulk crystallization (Figure 4(b)).

Approximately 500 nm diameter spherulites are observed at the surface of the sample after heat treatment at high temperature (Figure 4(a)). These spherulites must result from a dendritic growth,⁽²³⁾ as already reported in a similar system.⁽²⁴⁾ HT-ESEM observation confirms that these spherulites have been formed during the heat treatment and not during the cooling step. In parallel, the bulk of the LNS 25 glass-ceramic contains large spherulites the diameter of which is approximately $25\ \mu\text{m}$, as already reported in Ref. 25, pointing out an important difference between the surface and the bulk crystallization mechanism.

As (i) greater precipitation of nuclei is expected on the surface and (ii) crystallites' growth may be limited by neighbouring particles, a large number of crystallites can coalesce rapidly to form a large amount of spherulites with relatively limited size. Deeper in the glass-ceramic bulk, the nuclei precipitation is less intense and the growth of initial crystallites leads to larger spherulites.

Taking into account that the x-ray patterns indicate that the *c*-axis of the LiNbO_3 crystallites are perpendicular to the surface, we suppose that spherulites containing *c*-axis oriented crystallites are distributed in a radial fashion as already reported in Refs. 26, 27. On the surface, a fraction of incomplete spherulites might have accumulated perpendicularly to the surface during the heat treatment, leading to a very high *c*-axis orientation contribution. After polishing of the sample surface, we remove this contribution of incomplete spherulites and we only observe the complete spherulites that have grown in the sample bulk without any constraints due to close neighbours. Thus, this can explain that less preferential orientation along the *c*-axis is observed in the bulk. Those particular large spherulites might be at the origin of the shape of the macroscopic SHG signal. Further work will be undertaken to more deeply investigate the orientation of crystallites inside the spherulites and to correlate the macroscopic NLO to the precipitation of the spherulites.

Conclusion

The use of *in situ* techniques has enabled the characterization of the surface of LNS 25 glass-ceramic during the crystallization process. Precipitation of LiNbO_3 crystallites oriented along the *c*-axis starts at the glass transition temperature. The rearrangement of the distorted octahedral NbO_6 present in the glass into regular NbO_6 octahedra that are characteristic of the LiNbO_3 crystalline structure has been well estab-

lished by HT- μ -Raman spectroscopy. On the sample surface, 500 nm to 4 μ m diameter spherulites have been observed, their final size depending on heat treatment conditions. Furthermore, we suppose that there is an accumulation of incomplete spherulites perpendicular to the surface, with a radial distribution of c -axis oriented crystallites inside spherulites, at the sample surface. In the sample bulk, we can expect that similar crystallites form but the growth of complete spherulites is made easier due to limited interactions between neighbouring spherulites.

Acknowledgment

This work has been supported by Région Aquitaine (Advanced Materials in Aquitaine - LasINOF), Commissariat à l'Énergie Atomique and PICS-CNRS-5584/RFBR grant. The authors would also like to thank E. Lebraud and S. Péchev (ICMCB, CNRS) for carrying *in-situ* x-ray diffraction on the glass-ceramic samples.

References

1. Glass, A. M., Lines, M. E., Nassau, K. & Shiever, J. W. Anomalous dielectric behavior and reversible pyroelectricity in roller-quenched LiNbO₃ and LiTaO₃ glass. *Appl. Phys. Lett.*, 1977, **31**, 249–251.
2. Layton, N. M. & Smith, J. W. Pyroelectric Response in Transparent Ferroelectric Glass-Ceramics. *J. Am. Ceram. Soc.*, 1975, **58**, 435–437.
3. Smolenskii, G. A., Krainik, N. N., Khuchua, N. P., Zhdanova, V. V. & Mylinkova, I. E. The Curie Temperature of LiNbO₃. *Phys. Status Solidi b*, 1966, **13**, 309–14.
4. Abrahams, C., Redy, J. M. & Bernstein, J. L. Ferroelectric Lithium Niobate. 3. Single Crystal X-Ray Diffraction Study at 24. *J. Phys. Chem. Solids*, 1966, **27**, 997–1012.
5. Prapitpongwanich, P., Harizanova, R., Pengpat, K. & C. Rüssel, Nanocrystallization of ferroelectric lithium niobate in LiNbO₃-SiO₂ glasses. *Mater. Lett.*, 2009, **63**, 1027–1029.
6. Todorovic, M. & Radonjic, L. J. Lithium-Niobate Ferroelectric Material Obtained by glass Crystallization. *Ceram. Int.*, 1997, **23**, 55–60.
7. Gerth, K., Rüssel, C., Keding, R., Schleevoigt, P. & Dunken, H. Oriented Crystallisation of Lithium Niobate Containing Glass Ceramic in an Electric Field and Determination of the Crystallographic Orientation by Infrared Spectroscopy. *Phys. Chem. Glasses*, 1999, **40**, 135–139.
8. Sigaev, V. N., Golubev, N. V., Usmanova, I. Z., Stefanovich, S. Yu., Pernice, P., Fanelli, E., Aronne, A., Champagnon, B., Califano, V., Vouagner, D., Konstantinova, T. E. & Glazunova, V. A. On the Nature of the Second-Order Optical Nonlinearity of Nanoinhomogeneous Glasses in the Li₂O-Nb₂O₅-SiO₂ System. *Glass Phys. Chem.*, 2007, **33**, 97–105.
9. Sigaev, V. N., Golubev, N. V., Stefanovich, S. Yu., Komatsu, T., Benino, Y., Pernice, P., Aronne, A., Fanelli, E., Champagnon, B., Califano, V., Vouagner, D., Konstantinova, T. E. & Glazunova, V. A. Second-Order Optical Nonlinearity initiated in Li₂O-Nb₂O₅-SiO₂ and Li₂O-ZnO-Nb₂O₅-SiO₂ Glasses by Formation of Polar Centrosymmetric Nanostructures. *J. Non-Cryst. Solids*, 2008, **354**, 873–81.
10. Vigouroux, H., Fargin, E., Fargues, A., Le Garrec, B., Dussauze, M., Rodriguez, V., Adamietz, F., Mountrichas, G., Kamitsos, J. E., Lotarev, J. S. & Sigaev, V. Crystallization and Second Harmonic Generation of Lithium Niobium Silicate Glass Ceramics. *J. Am. Ceram. Soc.*, 2011, **94**, 2080–2086.
11. Lipovskii, A. A., Kaganovki, Y., Melehin, V. G., Tagantsev, D. K. & Yanush, O. V. Kerr phenomenon and Raman spectroscopy of one lithium-niobium-silicate glass-forming system. *J. Non-Cryst. Solids*, 2008, **354**, 1245–1249.
12. Graca, M. P. F. & Ferreira da Silva, M. G. Structural and electrical properties of SiO₂-Li₂O-Nb₂O₅ glass and glass-ceramics obtained by thermoelectric treatments. *J. Mater. Sci.*, 2007, **42**, 2543–2550.
13. Graca, M. P. F., Ferreira da Silva, M. G., Sombra, A. S. B. & Valente, M. A. Electrical characterization of SiO₂:LiNbO₃ glass and glass-ceramics using dc conductivity, TSDC measurements and dielectric spectroscopy. *J. Non-Cryst. Solids*, 2007, **353**, 4390–4394.
14. Dussauze, M., Fargin, E., Malakho, A., Rodriguez, V., Buffeteau, T. & Adamietz, F. Correlation of large SHG responses with structural characterization in borophosphate niobium glasses. *Opt. Mater.*, 2006, **28**, 1417–1422.
15. Cardinal, T., Fargin, E., Le Flem, G. & Leboiteux, S. Correlations between structural properties of Nb₂O₅-NaPO₃-Na₂B₄O₇ glasses and non-linear optical activities. *J. Non-Cryst. Solids*, 1997, **222**, 228–234.
16. Claus, R., Borstel, G., Wiesendanger, G. E. & Steffan, L. Z. Directional dispersion and assignment of optical phonons in lithium niobate. *Z. Naturforsch A*, 1972, **27**, 1187–1192.
17. Claus, R., Borstel, G., Wiesendanger, G. E. & Steffan, L. Z. Assignment of optical phonons modes in LiNbO₃. *Phys. Rev. B*, 1972, **6**, 4878–4879.
18. Ridah, A., Bourson, P., Fontana, M. D. & Malovichko, G. The composition dependence of the Raman spectrum and new assignment of the photons in LiNbO₃. *J. Phys. Condens. Matter*, 1997, **9**, 9687–9693.
19. Schaufele, R. F. & Weber, M. J. Raman Scattering by Lithium Niobate. *Phys. Rev.*, 1966, **152**, 705–708.
20. Repelin, Y., Husson, E., Bennani F. and Proust, C. Raman Spectroscopy of lithium niobate and lithium tantalite force field calculation. *J. Phys. Chem. Solids*, 1999, **60**, 819–825.
21. Dussauze, M., Kamitsos, E. I., Fargin, E. & Rodriguez, V. Structural Rearrangements and Second-Order Optical response in the Space Charge Layer of Thermally Poled Sodium-Niobium Borophosphate Glasses. *J. Phys. Chem. C*, 2007, **111**, 14560–14566.
22. Fuss, T., Ray, C. S., Kitamura, N., Makihara, M. & Day, D. E. Pressure induced nucleation in a Li₂O-SiO₂ glass. *J. Non-Cryst. Solids*, 2003, **318**, 157–167.
23. Granazy, L., Pusztai, T., Tegze, G., Warren, J. A. & Douglas, J. F. Growth and Form of Spherulites. *Phys. Rev. E*, 2005, **72**, 011605-1/011605-15.
24. Zeng, C., Tanaka, K., Hirao, K. & Soga N. Crystallization and glass formation in 50Li₂O-50Nb₂O₅ and 25Li₂O-25Nb₂O₅-50SiO₂. *J. Non-Cryst. Solids*, 1997, **209**, 112–121.
25. Prasad, N. S. & Varma, K. B. R. Evolution of ferroelectric LiNbO₃ phase in a reactive glass matrix (LiBO₂-Nb₂O₅). *J. Non-Cryst. Solids*, 2005, **351**, 1455–1565.
26. Alizadeh, P. & Marghussian, V. K. The effects of compositional changes on the crystallization behaviour and mechanical properties of diopside-wollastonite glass-ceramics in the SiO₂-CaO-MgO (Na₂O) system. *J. Eur. Ceram. Soc.*, 2000, **20**, 765–773.
27. McMillan, P. W. *Glass ceramics*, Academic Press, London, 1979.